Inverse modelling of core flood experiments for predictive models of sandstone and carbonate rocks

Senyou An[1], Nele Wenck[1], Sojwal Manoorkar[1], Steffen Berg[2], Conxita Taberner[2], Ronny Pini[3], Samuel Krevor[*1]

[1]Department of Earth Science and Engineering, Imperial College London, London, SW7 2AZ, UK

[2]Shell Global Solutions International B.V., Grasweg 31, 1031HW Amsterdam, The Netherlands

[3]Department of Chemical Engineering, Imperial College London, South Kensington, SW7 2BX, United Kingdom

Key Points:

- This paper demonstrates a workflow for creating predictive models of heterogeneous sandstone and carbonate rocks
- Multi parameter fitting of capillary pressure functions and permeability-capillary pressure correlations are introduced into the iterative modelling approach
- The new parameters are fit in a sequential iterative approach constrained against over fitting
- The developments lead to major improvements in the history matching and predictive capability of models for three carbonate and two sandstone rock samples samples with wide ranging heterogeneities

Corresponding author: Samuel Krevor, <s.krevor@imperial.ac.uk>

Abstract

Evidence from field-scale simulations and on-site observations suggests that multi-scale rock heterogeneities control subsurface fluid flow, and these must be characterised for accurate predictions of fluid migration, such as during CO_2 sequestration. Recent efforts have focused on continuum simulation-based inversion of laboratory observations with X-ray imaging, but models produced in this way have been limited in their predictive ability for highly heterogeneous rocks. We address the main challenges in this approach through the development of an algorithm that combines a number of significant advancements: the use of a 3-parameter capillary pressure model fitting, the implementation of spatial heterogeneity in absolute permeability, the constraint of history match iterations based on marginal error improvement, and more sophisticated image processing incorporating more of the experimental data in the calibration. We demonstrate the major improvement resulting from this workflow on five rocks (two sandstones and three carbonates), representing a range of heterogeneous properties, some of which could not be previously modeled. The algorithm results in physically representative 3D models of all the rock cores, reducing non-systematic error in both calibration and prediction of flow properties to a level comparable to the experimental uncertainty.

Plain Summary

Porous materials, both natural and man-made, exhibit spatial heterogeneity ranging from rock pores to the scales of geological units. Accurately characterising the impact of rock heterogeneity on hydrodynamic properties has been extensively studied but remains an open scientific question, particularly at the core scale of a few decimeters. This study demonstrates a new approach to effectively characterising the flow properties of highly heterogeneous rocks, including sandstone and carbonate rocks. This approach overcomes major barriers that previously prevented the succesful modelling of highly heterogeneous rocks. As a result, it is now possible to characterise multiphase flow property heterogeneity in a wide range of rock types.

1 Introduction

Accurately characterising subsurface multiphase flow in permeable rocks is critical for analysing a wide range of natural and engineering phenomena, such as environmental contaminant remediation, subsurface energy resource development, and carbon geosequestration for climate change mitigation. Difficulties in modeling the physical processes governing fluid flow can lead to inaccurate field-scale flow simulations. This issue is prominent at CO_2 storage sites, where scientific pilot and industrial demonstration projects have demonstrated unexpectedly rapid CO_2 migration in directions that are difficult to forecast and history match [*Halladay et al.*, 2018]. Heterogeneity in the multiphase flow properties, relative permeability and capillary pressure, has been identified as one cause of the unexpected flow phenomena observed at field sites [*Jackson and Krevor*, 2020; *Benham et al.*, 2021]. However, there are no established workflows to characterise these heterogeneities.

Core analysis techniques have been developed to characterise the flow properties of subsurface rocks, including porosity, absolute permeability, capillary pressure, and relative permeability [*Calhoun et al.*, 1949; *Jones and Roszelle*, 1978; *Ali*, 1997; *McPhee et al.*, 2015]. Since the 1970s, medical X-ray computed tomography has been used to image multiphase flow experiments, providing direct observations of the 3D distribution of porosity and fluid saturation at controlled flow conditions [*Withjack*, 1988]. Computer-based inverse modelling is standard practice to account for the effects of boundary conditions on the interpretation of relative permeability from core-flooding tests [*Archer and Wong*, 1973; *Nordtvedt et al.*, 1999; *Berg et al.*, 2021].

Inverse modeling using X-ray imagery of fluid saturation distributions in core floods has also been used to parameterise heterogeneous capillary pressure characteristics in one-dimensional and three-dimensional models [*Huang et al.*, 1995; *Egermann and Lenormand*, 2005; *Krause et al.*, 2011, 2013; *Kong et al.*, 2015; *Oh et al.*, 2015; *Jackson et al.*, 2018; *Hejazi et al.*, 2019; *Anto-Darkwah et al.*, 2023]. In these approaches, a model is calibrated by scaling spatially varying capillary pressure characteristic curves until observed and simulated saturations are matched within experimental uncertainty. These models were initially used for the interpretation of core flood tests [*Huang et al.*, 1995; *Egermann and Lenormand*, 2005]. A number of developments have improved the history match of models to observed saturation distributions, including multi-parameter fitting of capillary pressure curves [*Kurotori and Pini*, 2021; *Anto-Darkwah et al.*, 2023], the inclusion of variation in absolute permeability [*Krause et al.*, 2011], and the extension of the approach to hysteretic drainage and imbibition cycles [*Anto-Darkwah and Rabinovich*, 2022]. Expanding the focus beyond history matching observations, *Krause et al.* [2011, 2013] introduced an iterative history match

procedure that resulted in models with predictive capability for estimating upscaled flow properties. This was further developed and confirmed to result in physically representative models of sandstone rocks with modest heterogeneities [*Krause and Benson*, 2015; *Jackson et al.*, 2018; *Wenck et al.*, 2021]. These predictions can be important for identifying flow properties of heterogeneous rocks in the capillary-dominated flow regimes typical of subsurface reservoirs [*Jackson and Krevor*, 2020].

However, *Wenck et al.* [2021] showed that the iterative approach may fail to predict upscaled flow properties when applied to highly heterogeneous rocks. More heterogeneous rocks may exhibit strong variation in the form of local capillary pressure curves, and competing control of viscous and capillary forces on the fluid saturation distribution. Thus the iterative approach for more heterogeneous rocks may benefit from the inclusion of multi-parameter capillary pressure fitting, e.g., *Kurotori and Pini* [2021] and spatial variation in absolute permeability, e.g., *Krause et al.* [2013]. At the same time, the introduction of more model parameters brings with it an increased risk of overfitting that must be balanced against the systematic errors arising from underparameterisation.

In this work, we demonstrate that addressing these issues collectively results in a model construction workflow that can predict upscaled flow properties for sandstone and carbonate rocks with a broad range of heterogeneities. We build on the iterative approaches described in *Jackson et al.* [2018] and *Wenck et al.* [2021], while introducing flexibility in the capillary pressure characteristic curve, incorporating a third parameter to control the model curvature following the work of *Kurotori and Pini* [2021]. We reintroduce spatial variation in absolute permeability by utilizing a correlation with the capillary pressure. To mitigate potential model overfitting, we introduce a constraint on iterations, controlled by the marginal error reduction in the calibration. The resulting algorithm minimizes systematic errors to the extent that they are comparable to experimental uncertainty, both in model calibration (history match) and predictive capability of upscaled relative permeability. Analysis of the fit parameter distribution provides insights into the nature of the model calibrations concerning non-uniqueness and over-determination issues.

2 Methodology

2.1 Experimental datasets

Five experimental datasets were studied in this work. They were derived from two sandstone and three carbonate rock cores representing a range of heterogeneous properties. The datasets comprise observations from steady state core-flooding experiments that were previously performed and reported in *Reynolds and Krevor* [2015]; *Reynolds et al.* [2018]; *Manoorkar et al.* [2021]; *Wenck*

et al. [2021]. The experiments co-injected nitrogen and water or CO_2 and brine at high (HR) and low (LR) flow rates to obtain flow parameters in the viscous-limit (VL) and capillary-limit (CL) flow regimes, with capillary number in Table S6 of *Wenck et al.* [2021]. A medical X-ray CT scanner was used to take 3D X-ray images of the cores. Permeability and porosity of the rock cores were measured either or with both a permeameter and the core-flooding rig. Mercury intrusion porosimetry (MICP) experiments were conducted to obtain the capillary pressure characteristic curves.

The X-ray imagery obtained from each sample includes dry, water and gas saturated scans, as well as scans taken during the co-injection of fluids at ratios, or fractional flows. Each X-ray scan was repeated several (5-10) times to enable averaging and reduction of image noise. Both porosity (ϕ^i) and saturation (S_f^i) in each image voxel in the experiments were calculated in the standard way for medical X-ray CT imagery. The average grey values of the X-ray scans of the dry rock ($\mathcal{P}_d$), single phase saturated scans ($\mathcal{P}_w$ and $\mathcal{P}_{nw}$ for wetting and non-wetting phases, respectively), as well as partially saturated scans ($\mathcal{P}_f$, with subscript f for fractional flow) were recorded. The greyscale values of the CT scans were used to estimate the saturation of each phase at each grid block (i) using Equations 1,

$$\phi^i = (\mathcal{P}_w - \mathcal{P}_d)/\mathcal{P}_0 \,, \quad S_f^i = (\mathcal{P}_f - \mathcal{P}_{nw})/(\mathcal{P}_w - \mathcal{P}_{nw}), \tag{1}$$

where $\mathcal{P}_0$ is the difference in grey value between a fluid phase and air.

2.2 Model calibration

The first stage in the generation of the numerical model of the rock cores from X-ray imagery involves pre-processing the images. The images of the rock core are made of stacks of image slices. In each slice, we extracted the section comprising the rock core with a circle pattern by detecting the boundary of the core and rubber sleeve, as shown in Figure 1(a). The structural similarity index from *Wang et al.* [2003] was also calculated for different scans to further adjust the core extraction locations before averaging the images yielded from repeated scans to reduce the noise.

Next, numerical continuum models of the rock cores were created from the images. The grid of the models was created by meshing the raw X-ray CT imagery to element-based models by applying a 3D convolution matrix with a specified element size, Figure 1(b). The size of the element volume, Figure 1(c), chosen for the models was guided by combined consideration of the apparent length scales of rock heterogeneity, the experimental saturation precision, and the computational cost. The element volume must be large enough such that the assumption of a continuum property such as permeability is valid, while sufficiently small so that heterogeneities in these properties are captured

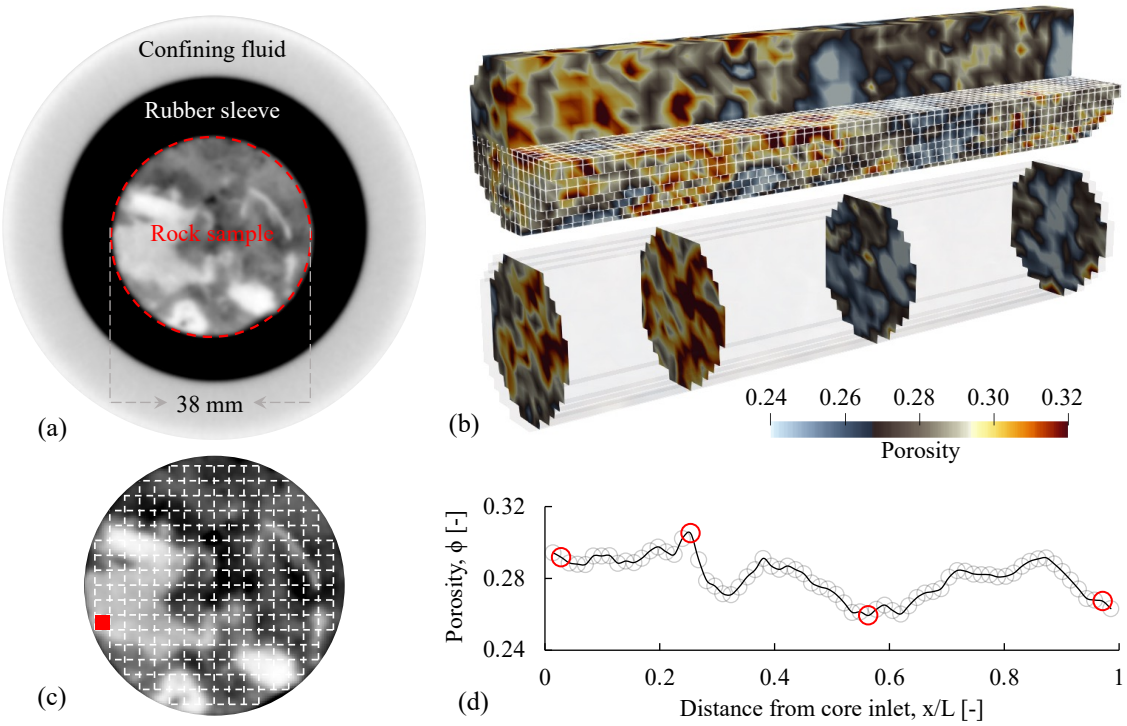

Figure 1. The upscaled core-scale structure. (a) Raw image from CT scanning with effective domain in the red circle. (b) 3D porosity field and the cross-sectional map. (c) The upscaled element volume concept (red square) and the meshed grey image. (d) The cross-sectional average porosity profile from inlet to outlet.

(See *Jackson et al.* [2018]). The size of the element volume for this work was chosen to be 2 mm [*Manoorkar et al.*, 2021; *Wenck et al.*, 2021].

The initial setup, depicted in Algorithm 1 and Figure S1 of Supplementary Information (S1), is followed by the image processing and upscaling of experimental parameters. The porosity field obtained from the X-ray imagery (Equation 1) was used to parameterise the model. The inlet flux and outlet pressure conditions of the simulation were intended to represent the experiments by using two buffer layers with high permeability and zero capillary pressure. To initialise the model, the hydrodynamic properties (e.g., permeability, capillary pressure) of local grid blocks were approximated based on the parameters of host and neighbouring grids, which we refer to as a cell unit in this work. As an alteration, the cell unit can also be implicitly assumed to be a slice of the rock core (especially layers perpendicular to the flow direction) through the assumption that the capillary pressure in each slice was constant. In the initial model setup, a prior measured capillary pressure curve (usually from MICP measurements) was assumed to represent the core-average parameter. The

experimental saturation (S_f^i) of the cell unit (rock core slice) is an observed parameter. Therefore, in each cell unit, the capillary pressures at distinct fractional flows can be estimated using the whole core capillary pressure curve and the phase saturation of the cell unit. Then, experimentally observed saturation fields within a cell unit at distinct fractional flows were used to estimate an initial capillary pressure - saturation relationship for each grid block. In summary, the initial parameterisation of heterogeneous capillary pressure characteristics is based on three observations: an *apriori* measured capillary pressure characteristic curve assumed to represent the rock core as a whole, the average saturation within each cell unit to constrain the capillary pressure in that cell unit, and the saturation distribution within the cell units to generate the various $P_c - S_w$ pairings comprising the capillary pressure characteristic curves. Subsequently, the capillary pressure characteristic curves were used as matching parameters in a sequential algorithm, described in detail below. We minimise the mismatch in observed and simulated local saturation using a capillary pressure function as the tuning parameter.

One of the main advancements highlighted in this work is the introduction of a multi-parameter fitting approach for local capillary pressure relationships. The model used in this work was proposed by *Li* [2004] based on the classic Brooks and Corey capillary pressure model [*Brooks and Corey*, 1966],

$$P_c = P_{\max}\left(1 - \left(1 - \alpha^{-\lambda}\right) S^*\right)^{-\frac{1}{\lambda}}, \tag{2}$$

where $\alpha = P_e/P_{\max}$ is the ratio of entry capillary pressure to the maximum capillary pressure, λ is a parameter related to the pore throat size distribution, and the wetting phase saturation normalised to an irreducible saturation, S_{wi}, is $S^* = (S_w - S_{wi})/(1 - S_{wi}) \in [0, 1]$.

The parameters used in the fitting are the entry pressure, P_e, the maximum capillary pressure, $P_{\max}$, which is the capillary pressure at the residual non-wetting phase saturation, and the model curvature λ which is related to the pore throat size distribution. We use a sequential approach in varying these parameters to fit the data to avoid non-uniqueness arising from the simultaneous coupling of multiple parameters. We first fit the entry capillary pressure while limiting any variation of the other parameters as an initial estimation. Then the maximum capillary pressure and curvature are subsequently varied by gradually increasing the range constraint. To mitigate the risk of over-fitting, a range limit is implemented when expanding the boundary conditions of fitting parameters does not improve the fitting accuracy. The first loop of Algorithm 1 in the SI iterates until the tuning results in a saturation distribution achieving the preset tolerance.

Subsequently, a second loop is carried out which is the same as the first loop, except that the absolute permeability is also varied for each grid block. Permeability is estimated for each grid block using a correlation with the porosity and capillary pressure curve developed by *Li et al.* [2021]. The correlation was based on a bundle of tubes and the classic Purcell-Burdine model [*Purcell*, 1949; *Burdine*, 1953; *Nakornthap and Evans*, 1986], Equation 3.

$$k = 10.66 \frac{\beta}{2n} (\sigma \cos\theta)^2 \phi^3 (1 - S_{wi})^3 \int_0^1 \frac{1}{P_c^2} dS^*. \tag{3}$$

Combining Equations 2 and 3, results in the basic form of the correlation for absolute permeability,

$$k = 10.66 \frac{\beta}{2n} (\sigma \cos\theta)^2 \phi^3 (1 - S_{wi})^3 \frac{1}{P_{max}^2} \frac{\lambda}{\lambda + 2} \frac{1 - \alpha^{-(\lambda+2)}}{1 - \alpha^{-\lambda}}. \tag{4}$$

A more general form of the function was then given by,

$$k = a_1 \phi^{a_2} (1 - S_{wi})^{a_3} \frac{1}{P_{max}^{a_4}} \left(\frac{\lambda}{\lambda + 2} \frac{1 - \alpha^{-(\lambda+2)}}{1 - \alpha^{-\lambda}} \right)^{a_5}. \tag{5}$$

Li et al. [2021] empirically fit the coefficients in Equation 5 using measurements made on 151 rock samples across a range of lithologies. In this work, the coefficients $a_{2\ldots5}$ were adopted from *Li et al.* [2021]. The value of a_1 for all grid blocks is shifted such that the absolute permeability of the whole core remains equal to the measured value. The updated absolute permeability is utilized in subsequent simulations and further affects the sequential capillary pressure fitting.

While considering relative permeability heterogeneity is a possibility, doing so would necessitate the imposition of more experimental constraints. Although models have been developed to correlate relative permeability to other properties, particularly the capillary pressure characteristics [*Li*, 2004], these models are less well validated relative to the capillary pressure - permeability relationships. In this work, the input relative permeability is the same for all grid blocks throughout the model.

3 Results and discussions

The results for the Estaillades Limestone sample are described in detail, followed by a discussion of the results for the other rocks. The properties of the sample (absolute permeability, open-source image data, MICP data, relative permeability, etc.) can be found in *Manoorkar et al.* [2021]; *Wenck et al.* [2021]. Using the modified X-ray image processing algorithm, about 82% of the sample volume is included in the numerical model, Figure 1. The experimental MICP data was fitted using Equation 2 to obtain the whole core reperesentative capillary pressure curve. The viscous limit

relative permeability curve was obtained by fitting a Chierici function [*Chierici*, 1984] to the high flow rate (20 mL/min) experimental data and used as input to the simulation.

After initialising the numerical model, iterations were carried out to match the saturation field from low flow rate experiments (0.5 mL/min). The matching results are shown in Figure 2 by visual comparison of saturation distributions in 1D and 3D, and by plot of simulated and observed saturation values for corresponding locations in the rock and model, respectively. The 3D distribution patterns of N_2 saturation are visually similar between the experiment and simulations, particularly the larger scale features. The slice averaged N_2 saturation profile at the final state is shown in Figure 2(b), and further shows that the fitting result is able to accurately capture the saturation distribution. The goodness of fit is quantified in the graph of Figure 2(a), showing the location by location comparison of simulated and observed saturations at all fractional flow stages. The data mostly falls within the experimental uncertainty. Experimental N_2 saturation and numerical values have a linear dependence with a Pearson correlation coefficient of 0.95.

The saturation distribution is the fitting target to construct the numerical model. The validation of the calibrated model comes from its use in predicting the observed relative permeability data for the experiment data at the low flow rate, and this is shown in Figure 2 (d). The experimentally derived datapoints are direct observations of the average saturation and relative permeability calculated from the observed pressure differential using Darcy's law, and do not use any correction for capillary end effects. We are, in essence, predicting the observables of the experiment with the simulation to validate our model. The deviation of the data and curves at low fluid flow rates from the data and corresponding simulation input obtained at high flow rate (black points and curve in Figure 2 (d) reflects the combined impact of heterogeneities in the rock, and capillary end effects. From the comparison, we can conclude that the low flow rate relative permeability is successfully predicted with a correlation coefficient of 0.98.

The proposed algorithm provides a way to characterise the absolute permeability and capillary pressure distribution in the decimeter-scale rock sample, and these results are shown in Figures 2(c), (e), and (f). Comparing Figures 2(c) and 1(b), we can observe the entry capillary pressure field has a positive relation with porosity distribution in this instance, although this is not imposed by the models. There is an imposed correlation between absolute permeability, capillary pressure, and porosity from Equation 5, and this can be seen in Figures 2(e) and (f).

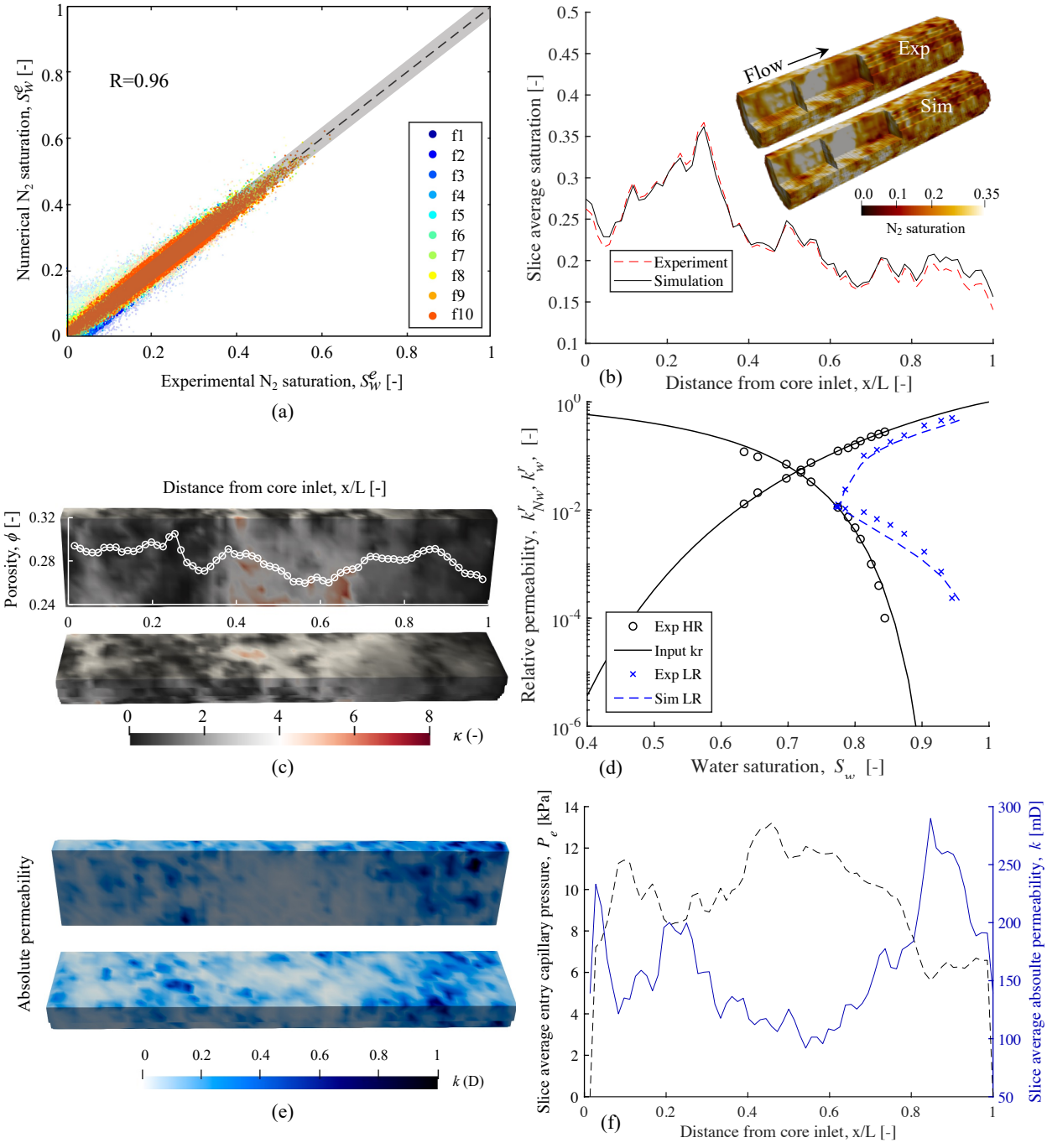

Figure 2. The results of the history matching, characterisation, and prediction for Estaillades Limestone sample. (a) The voxel saturation correlation plot comparing the experiment and the simulation based saturations. The grey bar shows the experimental uncertainty in the estimate of saturation from the imaging. (b) The cross-sectional average saturation from inlet to outlet at the final state, with 3D saturation distribution from CT scanning and simulation. (c) The characterisation of capillary heterogeneity using κ, with slice average porosity embedded. (d) The fitted relative permeability curves at a high flow rate for simulation input, and the comparison of simulation results and experimental curves at a low flow rate to estimate the prediction. (e) The 3D absolute permeability field in the characterisation domain. (g) The slice averaged entry capillary pressure (left y axial) and absolute permeability (right y axial) from inlet to outlet.

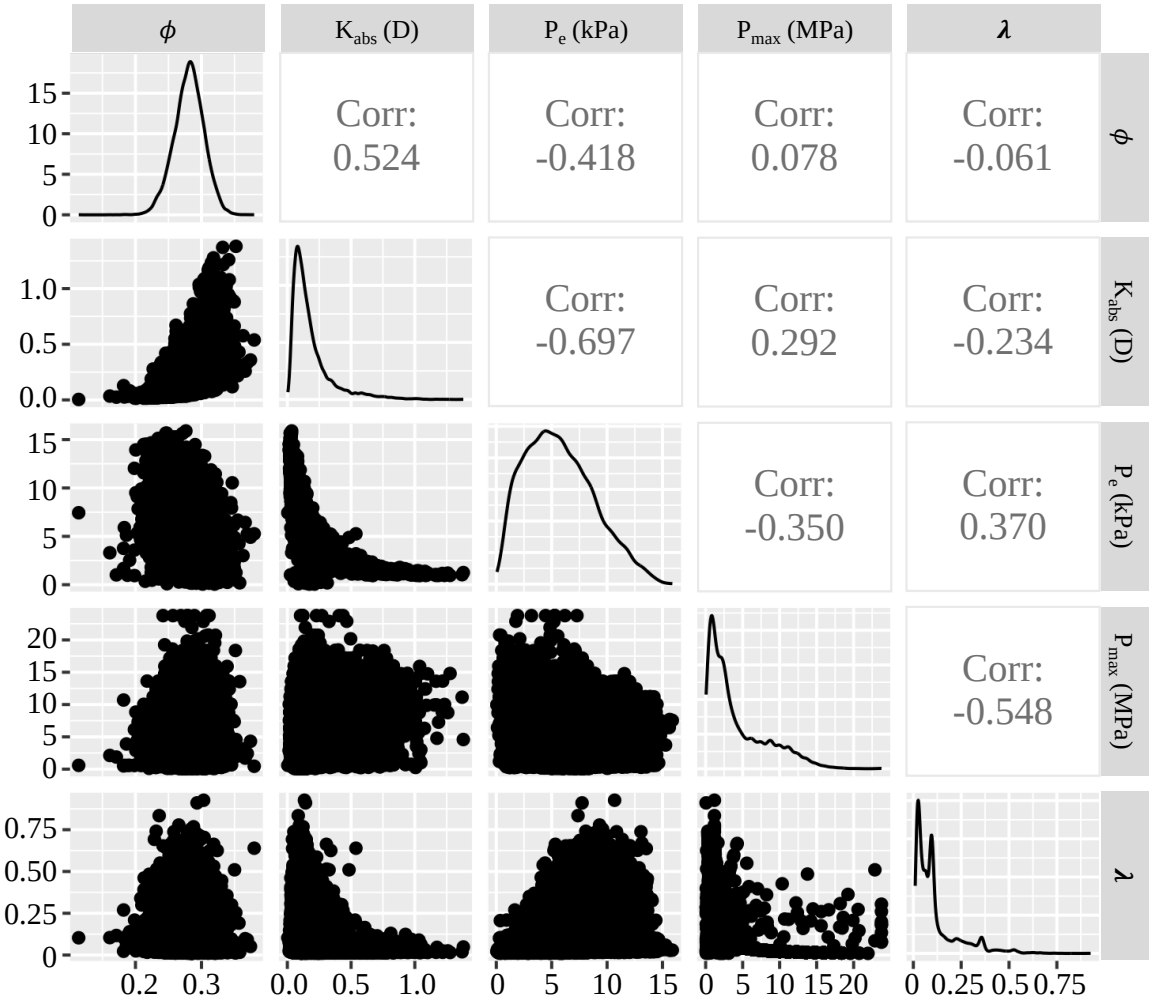

Figure 3. The correlation of characterised parameters (namely porosity, absolute permeability, entry capillary pressure, maximum capillary pressure, and the curvature λ) for Estaillades Limestone sample.

The algorithm in this study is a multi-parameter non-linear fitting process. To diagnose the potential for over-fitting, the cross correlation between porosity, absolute permeability, and capillary pressure parameters is calculated using GGally *Schloerke et al.* [2018]. These are shown in Figure 3. As expected, the entry capillary pressure is negatively correlated with porosity. Additionally, among all the correlations, the absolute permeability has stronger correlations with porosity, entry capillary, and even the curvature characterisation parameter (λ), as we derived the values using Equation 5. The few systematic errors (Figure 2(a)) and low cross correlations between parameters (Figure 3), other than the ones that are imposed, indicate that the model has high fidelity.

The results for the other four rocks, two sandstone (Bentheimer and Bunter) rocks and two carbonate (Edwards and Indiana) cores, are shown in Figure 4. The 3D porosity, capillary pressure and absolute permeability distributions are shown in Figure 5. The calibrated saturation distribution and the validating predictions of relative permeability indicate that the constructed models are able to represent the salient flow properties of the rocks.

We now describe the improvements made using this approach relative to past approaches. The sandstone rocks in this study were already successfully modelled using the approach of *Jackson et al.* [2018]; *Wenck et al.* [2021], and benefit marginally from the developments in this work. The Bentheimer sandstone is a shallow marine deposit, composed of ~95% fine to medium-grained quartz [*Peksa et al.*, 2015]. The sample is characterised by a layer parallel to the flow direction. The modelling of the Bentheimer benefit mostly from the improved image processing algorithm, i.e., incorporating a larger fraction of the imaged sample into the modelling. We successfully characterised the laminated structure parallel to the flow direction. The heterogeneity was also reflected in the capillary pressure and absolute permeability distribution. The other utilised sandstone, the Bunter sandstone, is composed mainly of subangular to subrounded quartz grains with a minor component of detrital K-feldspar, clay, as well as carbonate clasts, and exhibits characteristics of early diagenetic processes [*Brook et al.*, 2003]. From the characterisation, the chosen Bunter sample shows lamination perpendicular to the flow direction. Compared with other carbonate rocks, the two sandstone samples have orders of magnitude larger absolute permeability, and smaller variations in the capillary pressure characteristics.

In contrast to the sandstone rocks, modelling of the carbonate rocks was significantly improved relative to *Wenck et al.* [2021]. The Edwards Brown - from the Upper Cretaceous in Texas, USA - is mainly composed of ~90% dolomite and calcite, as well as ~10% quartz [*Lai et al.*, 2015]. The sample has decimeter-scale correlated porosity, with low-porosity regions near the outlet of the sample, as shown in Figure 5. This is the largest scale correlation among all samples. The capillary pressure and absolute permeability field also exhibit strong heterogeneity. The Estaillades rock from the Estaillades quarry (SE, France) is a Cretaceous bioclastic limestone with ~98% calcite, as well as ~2% dolomite, silica and other minerals [*Le Guen et al.*, 2007; *Manoorkar et al.*, 2021]. The characterisation (Figures 1 and 2) indicates that the Estaillades sample has centimeter-scale spatial correlation lengths in petrophysical parameters. Another carbonate sample (Indiana limestone) contains ~97% calcite, ~1.2% magnesium carbonate, and other minor components [*Churcher et al.*, 1991]. The porosity of the Indiana limestone rock has a millimeter-scale correlation length and the smallest variation among three carbonate samples.

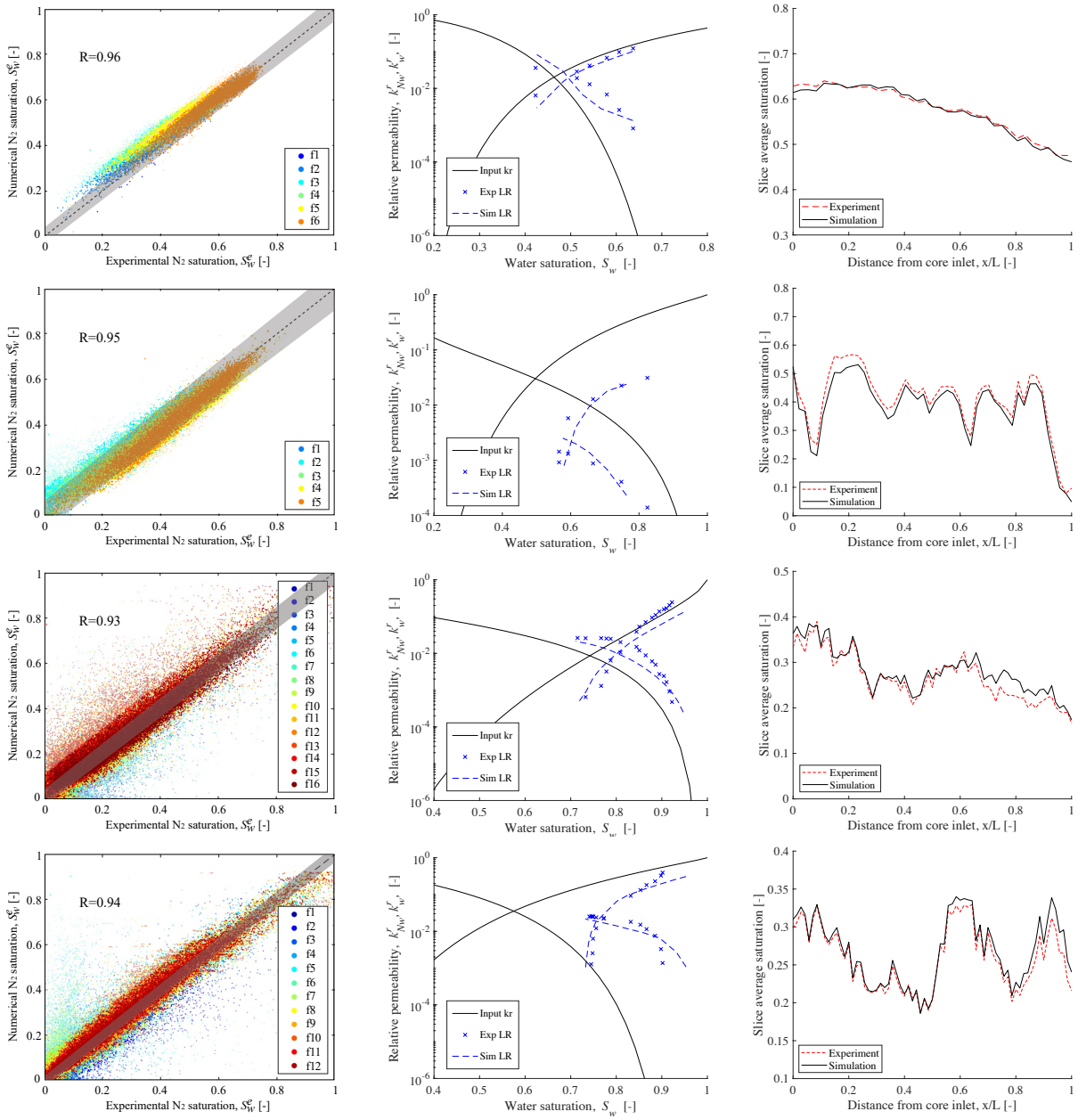

Figure 4. Rows from top to bottom represent Bentheimer sandstone, Bunter sandstone, Edwards carbonate, and Indiana carbonate rocks, respectively. Left column: The voxel saturation correlation plot comparing the experiment and simulated saturations from the calibration stage. Middle column: The fitted relative permeability curves at a high flow rate for simulation input, and the comparison of predicted simulation results and experimental curves at a low flow rate. Right column: the cross-sectional average saturation from inlet to outlet at the final fractional flow.

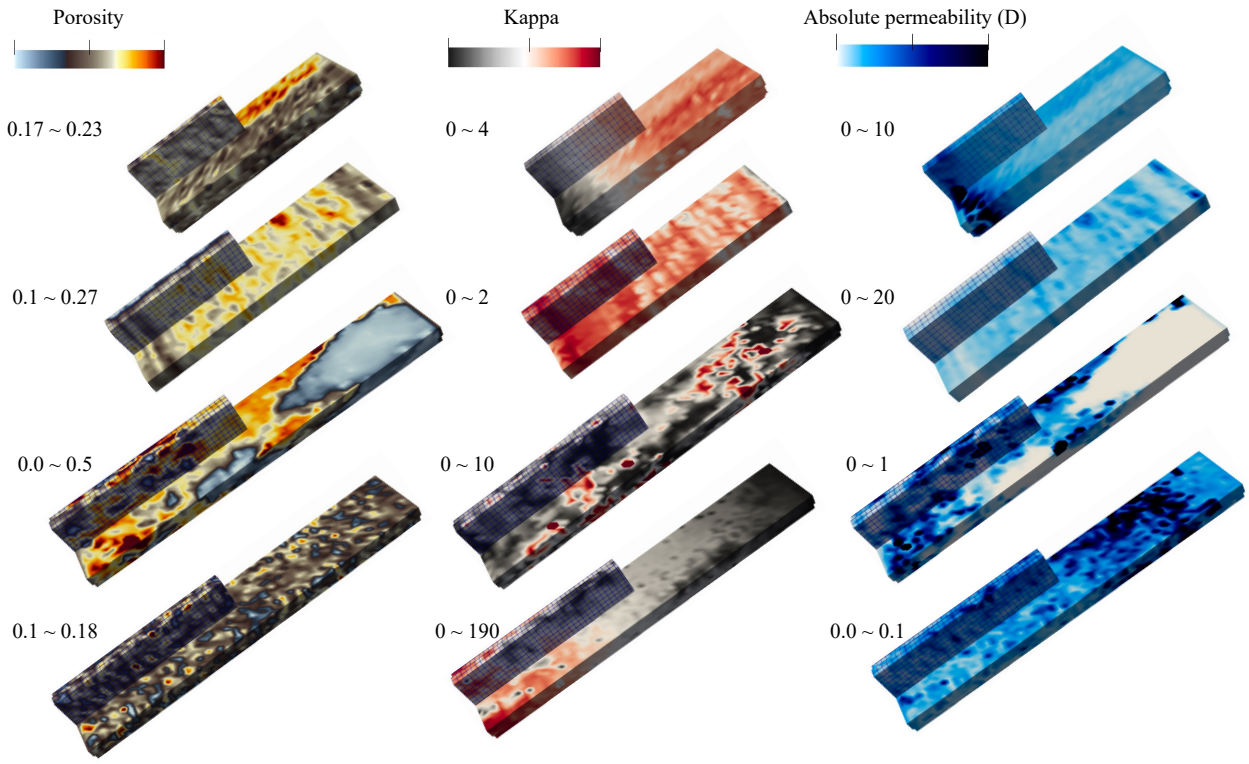

Figure 5. Rows from top to bottom represent Bentheimer sandstone, Bunter sandstone, Edwards carbonate, and Indiana carbonate rocks, respectively. Columns from left to right represent the 3D porosity, capillary entry pressure, and absolute permeability fields.

The improvements in generating physically representative models arose from all of the modifications introduced in this work. Through changes to the image processing algorithm, the size of the characterised domain for the rocks used in this study has been increased from ~50% to ~80%, compared to previously published results [*Jackson et al.*, 2018; *Wenck et al.*, 2021]. Although the expanded domain may lead to more numerical errors, the aligned images more accurately depict the experimental situation. A more general capillary pressure model with three fitting parameters was used to fit the capillary pressure curve in each local element. Figure S2 in SI illustrates that the local capillary pressure property was more reasonably fitted using a combination of entry capillary pressure, curvature, as well as maximum capillary. The correlation coefficient (R^2) increased from 0.75 to 0.92 for the example cell. The heterogeneous absolute permeability field also led to improvements in the relative permeability prediction. Finally, constraints on the number of iterations mitigated the potential for over fitting. At this stage, the proposed algorithm represents a versatile approach

to creating the physically representative models of a wide range of rock types needed for accurate modelling of field scale fluid migration processes.

Acknowledgments

We gratefully acknowledge funding from the Shell Digital Rocks II programme at Imperial College London.

Data Availability

The readers can find the input data and raw data of figures presented in the manuscript in the Mendeley repository with the doi: 10.17632/wwtpcsng76.1.

References

Ali, J. (1997), Developments in measurement and interpretation techniques in coreflood tests to determine relative permeabilities, in *Latin American and Caribbean petroleum engineering conference*, OnePetro.

Anto-Darkwah, E., and A. Rabinovich (2022), Modeling imbibition coreflooding in heterogeneous cores with sub-core scale hysteresis, *Advances in Water Resources*, *164*, 104,214.

Anto-Darkwah, E., T. Kurotori, R. Pini, and A. Rabinovich (2023), Estimating three-dimensional permeability distribution for modeling multirate coreflooding experiments, *Sustainability*, *15*(4), 3148.

Archer, J. S., and S. Wong (1973), Use of a reservoir simulator to interpret laboratory waterflood data, *Society of Petroleum Engineers Journal*, *13*(06), 343–347.

Benham, G. P., M. J. Bickle, and J. A. Neufeld (2021), Two-phase gravity currents in layered porous media, *Journal of Fluid Mechanics*, *922*, A7.

Berg, S., E. Unsal, and H. Dijk (2021), Non-uniqueness and uncertainty quantification of relative permeability measurements by inverse modelling, *Computers and Geotechnics*, *132*, 103,964.

Brook, M., K. Shaw, C. Vincent, and S. Holloway (2003), Gestco case study 2a-1 : storage potential of the bunter sandstone in the uk sector of the southern north sea and the adjacent onshore area of eastern england, this item has been internally reviewed but not externally peer-reviewed.

Brooks, R. H., and A. T. Corey (1966), Properties of porous media affecting fluid flow, *Journal of the irrigation and drainage division*, *92*(2), 61–88.

Burdine, N. (1953), Relative permeability calculations from pore size distribution data, *Journal of Petroleum Technology*, *5*(03), 71–78.

Calhoun, J. C., M. Lewis, and R. Newman (1949), Experiments on the capillary properties of porous solids, *Journal of Petroleum Technology*, *1*(07), 189–196.

Chierici, G. L. (1984), Novel relations for drainage and imbibition relative permeabilities, *Society of Petroleum Engineers Journal*, *24*(03), 275–276.

Churcher, P., P. French, J. Shaw, and L. Schramm (1991), Rock properties of berea sandstone, baker dolomite, and indiana limestone, in *SPE International Symposium on Oilfield Chemistry*, OnePetro.

Egermann, P., and R. Lenormand (2005), A new methodology to evaluate the impact of localized heterogeneity on petrophysical parameters (kr, pc applied to carbonate rocks, *Petrophysics-The SPWLA Journal of Formation Evaluation and Reservoir Description*, *46*(05).

Halladay, A., V. O. Bacci, S. O'Brien, and K. Hindriks (2018), Results from the second monitor das vsp at quest ccs, *Fifth CO2 Geological Storage Workshop*.

Hejazi, S. A. H., S. Shah, and R. Pini (2019), Dynamic measurements of drainage capillary pressure curves in carbonate rocks, *Chemical Engineering Science*, *200*, 268–284.

Huang, Y., P. Ringrose, and K. Sorbie (1995), Capillary trapping mechanisms in water-wet laminated rocks, *SPE Reservoir Engineering*, *10*(04), 287–292.

Jackson, S. J., and S. Krevor (2020), Small-scale capillary heterogeneity linked to rapid plume migration during co 2 storage, *Geophysical Research Letters*, *47*(18), e2020GL088,616.

Jackson, S. J., S. Agada, C. A. Reynolds, and S. Krevor (2018), Characterizing drainage multiphase flow in heterogeneous sandstones, *Water Resources Research*, *54*(4), 3139–3161.

Jones, S., and W. Roszelle (1978), Graphical techniques for determining relative permeability from displacement experiments, *Journal of Petroleum Technology*, *30*(05), 807–817.

Kong, X., M. Delshad, and M. F. Wheeler (2015), History matching heterogeneous coreflood of co2/brine by use of compositional reservoir simulator and geostatistical approach, *Spe Journal*, *20*(02), 267–276.

Krause, M., J.-C. Perrin, S. M. Benson, et al. (2011), Modeling permeability distributions in a sandstone core for history matching coreflood experiments, *Spe Journal*, *16*(04), 768–777.

Krause, M., S. Krevor, and S. M. Benson (2013), A procedure for the accurate determination of sub-core scale permeability distributions with error quantification, *Transport in porous media*, *98*(3), 565–588.

Krause, M. H., and S. M. Benson (2015), Accurate determination of characteristic relative permeability curves, *Advances in Water Resources*, *83*, 376–388.

Kurotori, T., and R. Pini (2021), A general capillary equilibrium model to describe drainage experiments in heterogeneous laboratory rock cores, *Advances in Water Resources*, *152*, 103,938.

Lai, P., K. Moulton, and S. Krevor (2015), Pore-scale heterogeneity in the mineral distribution and reactive surface area of porous rocks, *Chemical Geology*, *411*, 260–273.

Le Guen, Y., F. Renard, R. Hellmann, E. Brosse, M. Collombet, D. Tisserand, and J.-P. Gratier (2007), Enhanced deformation of limestone and sandstone in the presence of high fluids, *Journal of Geophysical Research: Solid Earth*, *112*(B5).

Li, C., W. Dai, B. Luo, J. Pi, Y. Liu, and Y. Zhang (2021), New fractal-dimension-based relation model for estimating absolute permeability through capillary pressure curves, *Journal of Petroleum Science and Engineering*, *196*, 107,672.

Li, K. (2004), Generalized capillary pressure and relative permeability model inferred from fractal characterization of porous media, in *SPE Annual Technical Conference and Exhibition*, OnePetro.

Manoorkar, S., S. J. Jackson, and S. Krevor (2021), Observations of the impacts of millimeter-to centimeter-scale heterogeneities on relative permeability and trapping in carbonate rocks, *Water Resources Research*, *57*(4), e2020WR028,597.

McPhee, C., J. Reed, and I. Zubizarreta (2015), *Core analysis: a best practice guide*, Elsevier.

Nakornthap, K., and R. D. Evans (1986), Temperature-dependent relative permeability and its effect on oil displacement by thermal methods, *SPE Reservoir Engineering*, *1*(03), 230–242.

Nordtvedt, J., H. Urkedal, E. Ebeltoft, K. Kolltveit, E. Petersen, A. Sylte, and R. Valestrand (1999), The significance of violated assumptions on core analysis results, in *Proc. Symp. SCA International Symposium, SCA*, vol. 9931.

Oh, J., K.-Y. Kim, W. S. Han, E. Park, and J.-C. Kim (2015), Migration behavior of supercritical and liquid co2 in a stratified system: Experiments and numerical simulations, *Water Resources Research*, *51*(10), 7937–7958.

Peksa, A. E., K.-H. A. Wolf, and P. L. Zitha (2015), Bentheimer sandstone revisited for experimental purposes, *Marine and Petroleum Geology*, *67*, 701–719.

Purcell, W. (1949), Capillary pressures-their measurement using mercury and the calculation of permeability therefrom, *Journal of Petroleum Technology*, *1*(02), 39–48.

Reynolds, C., and S. Krevor (2015), Characterizing flow behavior for gas injection: Relative permeability of co2-brine and n2-water in heterogeneous rocks, *Water Resources Research*, *51*(12), 9464–9489.

Reynolds, C. A., M. J. Blunt, and S. Krevor (2018), Multiphase flow characteristics of heterogeneous rocks from co 2 storage reservoirs in the united kingdom, *Water Resources Research*, *54*(2),

729–745.

Schloerke, B., J. Crowley, D. Cook, F. Briatte, M. Marbach, E. Thoen, A. Elberg, and J. Larmarange (2018), Ggally: Extension to 'ggplot2', *R package version*, *1*(0).

Wang, Z., E. P. Simoncelli, and A. C. Bovik (2003), Multiscale structural similarity for image quality assessment, in *The Thrity-Seventh Asilomar Conference on Signals, Systems & Computers, 2003*, vol. 2, pp. 1398–1402, Ieee.

Wenck, N., S. J. Jackson, S. Manoorkar, A. Muggeridge, and S. Krevor (2021), Simulating core floods in heterogeneous sandstone and carbonate rocks, *Water Resources Research*, *57*(9), e2021WR030,581.

Withjack, E. (1988), Computed tomography for rock-property determination and fluid-flow visualization, *SPE formation evaluation*, *3*(04), 696–704.